



# Nano-silicon/graphite composites caged by mesophase pitch-derived carbon as anode materials for stable lithium storage

Zhongtao Zhao<sup>1,2</sup> · Liang Ye<sup>1,2</sup> · Xiaolu Li<sup>1,2</sup> · Xianfeng Yang<sup>1,2</sup> · Shuguang Chen<sup>1,2</sup> · Peng Liu<sup>1,2</sup> · Jiangrong Kong<sup>1,2</sup>

Received: 20 March 2024 / Revised: 2 June 2024 / Accepted: 7 June 2024 / Published online: 13 June 2024  
© The Author(s), under exclusive licence to Springer-Verlag GmbH Germany, part of Springer Nature 2024

## Abstract

The development of silicon/graphite composites is a feasible solution for improving the short cycling life of Si-based anodes. However, unsatisfactory solid interfaces and structural integrity impede the achievement of the anticipated electrochemical performance. Herein, naphthalene-based mesophase pitch is used as the carbon precursor to wrap nano-Si/artificial graphite (AG) composites through an impregnation-carbonization route. Structural characterization revealed that the pyrolyzed carbon formed graphitic and porous carbon cages, which not only promoted the transport of charge carriers but also mitigated the expansion of Si particles. After 500 charge–discharge cycles at a high current density of 1000 mA g<sup>-1</sup>, the anode material with a Si/graphite/pitch mass ratio of 2:5:10 achieved a specific capacity of 432 mAh g<sup>-1</sup> and a coulombic efficiency of 99.5%. Considering the facile manufacturing technique, good cycling stability, and rate capability, Si/graphite/C anode materials possess promising industrialization prospects for next-generation lithium-ion batteries.

**Keywords** Lithium-ion batteries · Anode materials · Silicon/graphite composites · Mesophase pitch · Carbon cage

## Introduction

The use of next-generation lithium-ion batteries (LIBs) is expected to reduce fluctuations in renewable energy sources, such as wind and solar and energy, and increase the endurance of electric vehicles (EVs). There is an urgent need to develop high-capacity electrode materials to meet the increasing energy storage demands of LIBs [1, 2]. Silicon is recognized as the most promising substitute for commercial graphite anodes due to its dramatic gravimetric capacity (3579 mAh g<sup>-1</sup> at room temperature) and abundant resources [3–6]. However, Si-based anodes are subject to sluggish

kinetics because of their intrinsically low conductivity and lithium-ion diffusion coefficient. Moreover, the lithiation/delithiation process of the anode is often accompanied by a drastic volume change (> 300%) [7], resulting in the pulverization of Si particles and the uncontrolled regeneration of the solid electrolyte interphase (SEI). The structural evolution of the anode increases the charge transfer resistance and electrolyte consumption and thereby leads to low coulombic efficiency and short cycle life [8–11].

Si/graphite hybrid anode materials have great development prospects because they can be generated from the cost-effective and mature manufacturing techniques of graphite anode materials. Furthermore, the excellent conductivity and flexibility of graphite can offset the inherent deficiencies of Si-based materials in terms of electronic transport and volumetric strain. Currently, feasible industrial solutions for preparing Si/graphite hybrid materials include ball-milling [12, 13], mechanical pressing [14], and spray-drying [15, 16]. However, a common problem of the above methods is the rigid contact between Si particles and graphite flakes, which is unfavorable for charge transfer and stress conduction. In this regard, Si/graphite composites are often modified with pyrolytic carbon coatings. The coating layer can not only buffer the volume change of silicon, but also improve the structural integrity and stability.

Zhongtao Zhao and Liang Ye have contributed equally to this work.

✉ Peng Liu  
liupengmse@csust.edu.cn

✉ Jiangrong Kong  
kongjr@csu.edu.cn

<sup>1</sup> School of Materials Science and Engineering, Changsha University of Science and Technology, Changsha 410114, People's Republic of China

<sup>2</sup> Hunan Provincial Key Laboratory of Efficient and Clean Utilization of Manganese Resources, College of Chemistry and Chemical Engineering, Central South University, Changsha 410083, People's Republic of China

Pitch is a widely applicable precursor for carbon-based materials because of its high carbon yield and low cost. For example, Xu et al. [17] developed a scalable method to fabricate kilogram-scale graphite-Si-C/TiO<sub>2</sub> composites (GSCTs) via liquid-phase self-assembly combined with mechanical fusion and solid-phase sintering treatment. Choi et al. [18] reported that pitch-coated silicon nanolayer-embedded graphite exhibited excellent capacity retention of 81.9% after 200 cycles. Hsu et al. [19] added nanosized silicon to the surface of graphitic mesocarbon microbeads (MCMB) and then applied a pitch coating to the shell via a high-temperature carbonization process. After the 500th cycle, the capacity of the Si/MCMB/C material still remains at 650 mAh g<sup>-1</sup>. Liu et al. [20] prepared a carbon-encapsulated composite of graphite@nano-Si by rapid coating of pitch. The graphite@Si@C composite exhibited excellent electrochemical performance with an initial reversible charge capacity of 502.5 mAh g<sup>-1</sup>, a coulombic efficiency of 87.5%, and a capacity retention of 83.4% after 400 cycles. Phadatare et al. [21] anchored Si nanoparticles on nanographite flakes through an aerogel fabrication route and achieved a specific capacity of 455 mAh g<sup>-1</sup> after the 200th cycle with a coulombic efficiency of 97% at a current density of 100 mA g<sup>-1</sup>. However, the specific capacity of pitch-derived carbon is less than that of silicon. The modification of Si/graphite composites with pitch is worthy of further exploration to enhance the collaborative advantage of lithium storage capacity and structural stability.

In this work, we provide a promising method for the batch production of Si/artificial graphite (AG)/C anode materials. Herein, naphthalene-based mesophase pitch was used as the precursor for carbon coatings. Compared to conventional pitch, mesophase pitch contains more polyaromatic hydrocarbons, which can self-organize into layered structures during pyrolysis. Our previous study [22] showed that an array of mesophase monolayers could be converted into graphene-like sheets via a carbonization process. Accordingly, pitch-derived carbon can serve as a cage that wraps nano-Si and graphite to stabilize the electrode structure and facilitate lithium-ion diffusion.

## Experimental

### Materials preparation

Nanoscale silicon with an average particle size of 30 nm (Qinghe Chuangying Metal), artificial graphite (AG, Chenzhou Botai Ultrafine Graphite), and naphthalene-based mesophase pitch (Jining Keneng New Carbon Materials) were mixed at mass ratios of 2:5:6, 2:5:8, 2:5:10, and 2:5:12 respectively. The raw materials were dispersed in carbon tetrachloride (Shanghai Macklin Biochemical Technology)

at 55 °C for 1 h with continuous stirring. After drying in an oven at 60 °C for 8 h, the as-received precursors were calcined at 800 °C under an ultrapure nitrogen atmosphere for 4 h in a furnace to obtain the anode materials (denoted as SGP-6, SGP-8, SGP-10, and SGP-12). Furthermore, a Si/graphite composite (SGP-0) was also employed as the anode material for comparison.

### Physical characterization

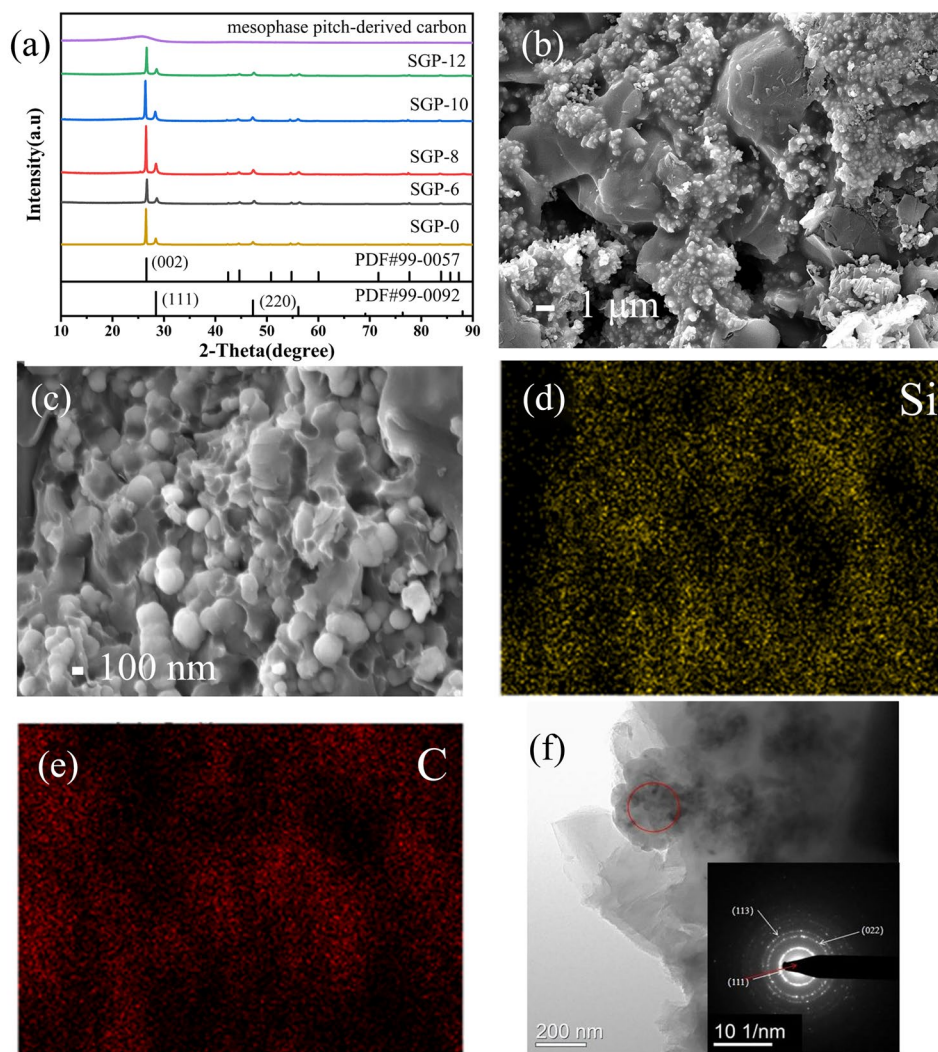
The crystal phase of the samples was identified using a D8 Advance X-ray diffractometer (XRD Bruker) in the 2θ range from 10° to 90°. The surface morphology and elemental composition of the samples were analyzed using a Quanta 250 scanning electron microscope coupled with an energy dispersive spectrometer (SEM and EDS, Nippon Electronics). The crystal microstructure of the anode material was characterized using a Tecnai F30 transmission electron microscope (TEM, FEI).

### Electrochemical measurements

The anode material was mixed with the conductive agent, Super P carbon black (~40 nm in size, Cyber Electrochemical Materials), and the binder, carboxymethyl cellulose (CMC, Sigma-Aldrich) to form an anode slurry at a weight ratio of 8:1:1, wherein the binder was configured as an aqueous solution with a mass fraction of 1.1%. The slurry was uniformly bladed on a copper foil. After drying in a vacuum oven at 110 °C for 6 h, the processed copper foil was cut into circular electrodes 12 mm in diameter. The loading of the active material on each electrode was approximately 0.57 mg cm<sup>-2</sup>. The CR2025 cells were assembled in an argon protected glovebox, using Li foil as the counter electrode, Celgard 2325 as the lithium-ion exchange membrane, and 1 M LiPF<sub>6</sub> in diethyl carbonate and ethylene carbonate (1:1 vol%) with 5% fluoroethylene carbonate (FEC) as the electrolyte. The full cell performance was evaluated using LiNi<sub>0.8</sub>Co<sub>0.1</sub>Mn<sub>0.1</sub>O<sub>2</sub> (NCM811, Hunan Changyuan Lico Co., Ltd) as the cathode material, with a loading of approximately 2.48 mg cm<sup>-2</sup> on each electrode. The ratio of the anode capacity to the cathode capacity (the N/P ratio) was set at 1.04.

Galvanostatic charge-discharge tests were performed using a CT2001A Battery Testing System (Wuhan Land Electronics) in a voltage range of 0.01–3.00 V (vs. Li/Li<sup>+</sup>). Cyclic voltammetry (CV) in the voltage range of 0.01–3.00 V (vs. Li/Li<sup>+</sup>) and electrochemical impedance spectroscopy (EIS) in the frequency range of 100 kHz–0.01 Hz were carried out using a DH7001 electrochemical workstation (Donghua Analysis Instruments).

**Fig. 1** **a** XRD patterns of mesophase pitch-derived carbon and Si/graphite/C materials, morphology, and elemental distribution of the SGP-10 anode material; **b** low-resolution SEM image; **c** high-resolution SEM image; **d** EDS mapping of Si; **e** EDS mapping of C; **f** TEM image with the inset SAED image



## Results and discussion

XRD patterns of the mesophase pitch-derived carbon and the Si/graphite/C composites are shown in Fig. 1a. The pitch-derived carbon presents a slight diffraction peak corresponding to the (002) crystal plane of the graphite. The diffraction peaks of the Si/graphite/C materials are highly consistent with those of the standard PDF cards of graphite (#99–0057) and silicon (#99–0092). The intensity of the (002) peak first increases and then decreases with increasing pitch-derived carbon content. It is suggested that the degree of graphitization will not decrease unless the mass fraction of pyrolytic carbon is too high. However, the characteristic peaks of silicon imply that the nano-silicon particles are not enclosed by pyrolytic carbon.

SEM images of the Si/graphite/C material (SGP-10) are shown in Fig. 1b–c. The carbon layer does not appear as a dense coating, but rather as a cage-like porous structure. Moreover, the Si nanoparticles are embedded in the carbon

coatings on the graphite flakes. This well-defined structure not only suppresses the volume expansion of nano-silicon, but also shields graphite from co-intercalation with solvent molecules. EDS mapping images (Fig. 1d–e) exhibit uniform elemental distributions of silicon and carbon, which benefits from the sufficient dispersion of the raw materials in the carbon tetrachloride solvent. The HR-TEM image in the TEM image (Fig. 1f) shows that the mesophase pitch-derived carbon encapsulating the silicon nanoparticles is supported by the graphite matrix. It can be inferred that the carbon cage facilitates the diffusion of lithium ions and improves the combination of silicon and graphite. As a result, the exfoliation or aggregation of silicon nanoparticles can be alleviated, which ensures the structural stability during charge–discharge cycles. The selected-area electron diffraction (SAED) pattern of the as-synthesized SGP-10 demonstrates that the diffraction rings are composed of discrete spots corresponding to the (111), (022), and (113) crystal planes of the silicon phase.

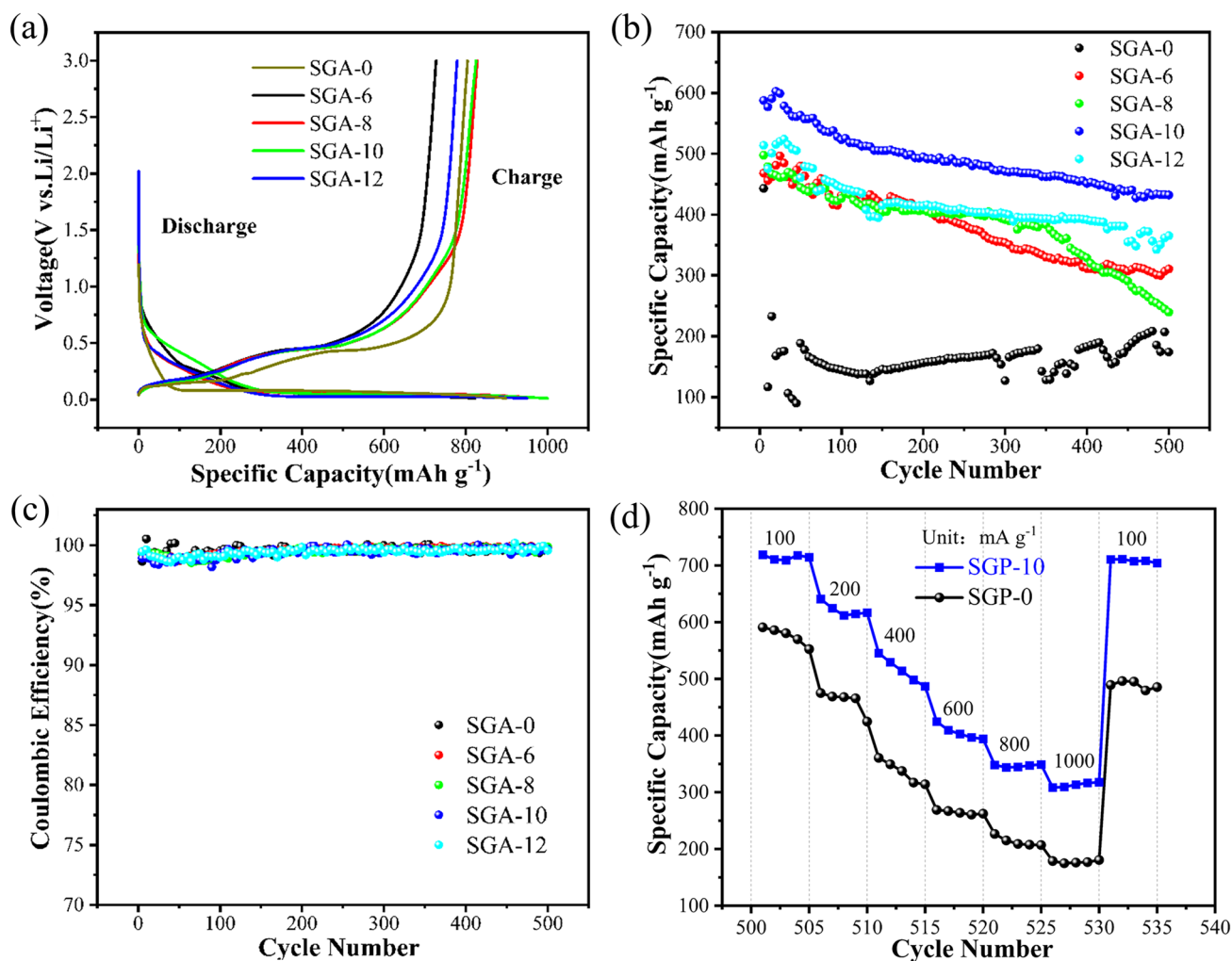


**Fig. 2** Electrochemical performance of Si/graphite and Si/graphite/C anode materials. **a** Galvanostatic charge–discharge curves at 100 mA g<sup>-1</sup> during the first cycle. **b** Cycling performance. **c** Coulombic efficiency. **d** Rate performance after cycle test

Figure 2a shows the galvanostatic charge–discharge curves of the Si/graphite and Si/graphite/C anode materials at a current density of 100 mA g<sup>-1</sup> during the first cycle. During discharge, the steep slope between 0.2 and 0.6 V indicates the formation of solid-electrolyte interphase (SEI) film [23]. Additionally, the long voltage platform around 0.2 V not only forms Li<sub>x</sub>Si alloy, but also includes the formation of LiC<sub>6</sub> [24]. All the anodes show two charge plateaus at 0.2 and 0.5 V vs. Li/Li<sup>+</sup>, corresponding to the delithiation reactions of graphite and silicon respectively. The discharge specific capacities of the SGP-8 and SGP-10 anode materials almost reach 1000 mAh g<sup>-1</sup> via pyrolytic carbon modification. The initial coulombic efficiencies (ICEs) of the Si/graphite/C anodes are 88.4%, 83.0%, 82.6%, and 82.0% respectively. Compared to the Si/graphite material (SGP-0: 90.0%), the slightly lower ICEs of the Si/graphite/C anode materials are attributed to the SEI lithium consumption of the

carbon cage with the high surface area. Nevertheless, the ICE values in this work are comparable to those reported in recent literature [25–27].

The cycling performance curves of the Si/graphite and Si/graphite/C anode materials at a current density of 1000 mA g<sup>-1</sup> are presented in Fig. 2b–c. The initial reversible capacity of the SGP-0 anode without modification by pitch carbon is 443 mAh g<sup>-1</sup>. After 500 cycles, the reversible capacity of the SGP-0 anode is 200 mAh g<sup>-1</sup>. In contrast, the Si/graphite/C anodes show more stable lithium storage performance. For example, the SGP-10 anode exhibits a reversible capacity of 432 mAh g<sup>-1</sup> and a coulombic efficiency of 99.5% in the 500th cycle. The improvement in cycling performance benefits from the fast diffusion paths of lithium ions constructed by the pitch carbon. Furthermore, the carbon cage can firmly anchor the Si nanoparticles on the surface of graphite and prevent pulverization of the active materials.



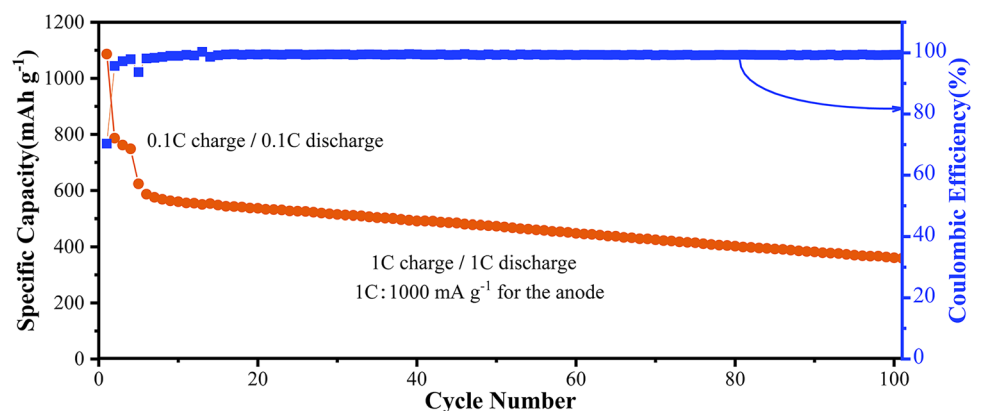
**Table 1** Comparison of electrochemical performance for Si/C anode materials in LIBs

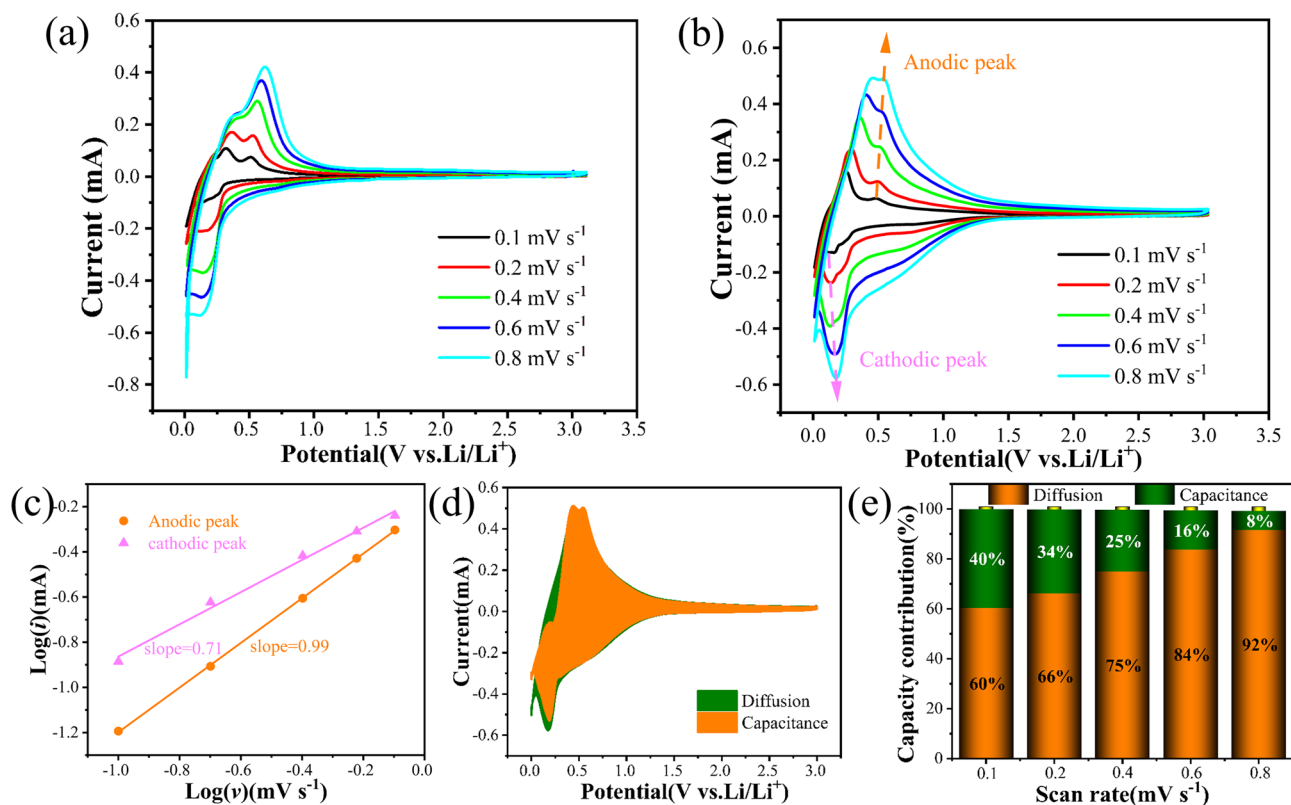
Sample	Initial discharge capacity (mAh g <sup>-1</sup> )	ICE	Cycles/capacity retention/current density	Rate capability (mAh g <sup>-1</sup> )	Method
SGP-10 (this work)	1000 at 0.1 A g <sup>-1</sup>	82.0%	500/73.6%/1 A/g	314 at 1A g <sup>-1</sup> (after long-term cycle test)	Impregnation Carbonization
Si/C/CNS [23]	1110 at 0.1 A g <sup>-1</sup>	70%	500/87.8%/1A/g	283 at 10A g <sup>-1</sup>	Template method Carbonization
Si/void/C/CNFs [24]	1194 at 0.1 A g <sup>-1</sup>	75.8	100/69.3%/0.1 A/g	317 at 1A g <sup>-1</sup>	Template method Electrospinning technique Carbonization
Si/G/C-CVD [28]	762 at 0.1 A g <sup>-1</sup>	79%	155/91%/0.1 A/g	262 at 1.6A g <sup>-1</sup>	Mechanical mixing Carbonization Chemical vapor deposition
Si/IIC [29]	1259 at 0.1 A g <sup>-1</sup>	67.2%	500/99%/0.1 A/g	558 at 1.2 A g <sup>-1</sup>	Ultrasound mixing Carbonization
S180[30]	602 at 0.1 A g <sup>-1</sup>	82.3%	100/71.5%/1A/g	279 at 2A g <sup>-1</sup>	Mechanical mixing Carbonization
GSCC [31]	1450 at 0.1 A g <sup>-1</sup>	78%	100/73%/0.2 A/g	400 at 2A g <sup>-1</sup>	Ball milling Spray drying Carbonization
PC/Np-Si [32]	2000 at 0.2 A g <sup>-1</sup>	78%	300/80%/1A/g	–	Chemical etching Impregnation Carbonization
G/Si/C [33]	574 at 0.1 A g <sup>-1</sup>	87.5%	400/83.4%/0.1A/g	120 at 2A g <sup>-1</sup>	Spray drying Carbonization

Figure 2d shows the rate capabilities of the Si/graphite and Si/graphite/C anode materials at current densities ranging from 100 to 1000 mA g<sup>-1</sup> after the cycle test. Both the SGP-0 and SGP-10 anodes display high capacities at lower current densities. When the current density increases to 1000 mA g<sup>-1</sup>, the reversible capacity of the SGP-10 anode is 300 mAh g<sup>-1</sup>, higher than that of the SGP-0 anode (170 mAh g<sup>-1</sup>). When the current density returns to 100 mA g<sup>-1</sup>, the reversible capacity of the SGP-10 anode can be restored to the initial capacity. The comparative study demonstrates that the Si/graphite/C materials possess rapid charge–discharge capability even after long-term cycling, benefiting from the reduction of Si/graphite interfacial resistance and the increasing ionic/

electronic conductivities. Table 1 summarizes some of the previous studies on silicon/carbon anode materials for lithium-ion batteries. Compared with these efforts, the SGP-10 composite exhibits competitive electrochemical performance. Additionally, the simple preparation method is suitable for mass production.

The cycling performance of SGP-10||NCM811 full cell is shown Fig. 3. The initial 4 charge–discharge cycles were run at 0.1 C, and the subsequent cycling test was carried out at 1C (1000 mA g<sup>-1</sup> for the anode). After 100 cycles, the SGP-10 anode shows a reversible capacity of 359.6 mAh g<sup>-1</sup> with a capacity retention of 58%. The capacity fading of the full cell is mainly caused by the thick film of NCM811 cathode that restricts the diffusion of lithium ions.

**Fig. 3** Cycling performance of a full cell pairing the SGP-10 anode with an NCM811 cathode



**Fig. 4** Cyclic voltammograms of the anode materials at various scan rates within a potential range of 0.01–3.00 V (vs. Li/Li<sup>+</sup>); **a** SGP-0; **b** SGP-10; **c**  $\log(i)$ - $\log(v)$  plots of SGP-10 at various scan rates from 0.1 to 0.8 mV s<sup>-1</sup>. **d** Area plot of the capacity contribution of the pseudo-

capacitance and diffusion at a CV scan rate of 0.8 mV s<sup>-1</sup>. **e** Capacity contribution of the SGP-10 anode at various scan rates from 0.1 to 0.8 mV s<sup>-1</sup>

Figure 4a–b shows cyclic voltammograms of the SGP-0 and SGP-10 anode materials at different scan rates. The two typical peaks at around 0.02 and 0.15 V during cathodic scanning can be explained by the generation of Li<sub>x</sub>Si alloy phases. Besides, the peak around 0.2 V could be attributed to the insertion of Li<sup>+</sup> into the artificial graphite and pitch-derived carbon [31, 34]. The reversibility of the electrode reaction can be described by comparing the potential difference between the oxidation and reduction peaks. As shown in Fig. 4a–b, the potential difference reduction peak of the SGP-10 anode is obviously lower than that of the SGP-0 anode at the same scan rate, reflecting the lower polarization for both the lithiation and delithiation reactions. In addition, the relationship between peak current ( $i$ ) and scan rate ( $v$ ) in the CV test curve can be expressed by Formulas (1) or (2) [13]:

$$i = av^b \quad (1)$$

$$\log(i) = b\log(v) + \log(a) \quad (2)$$

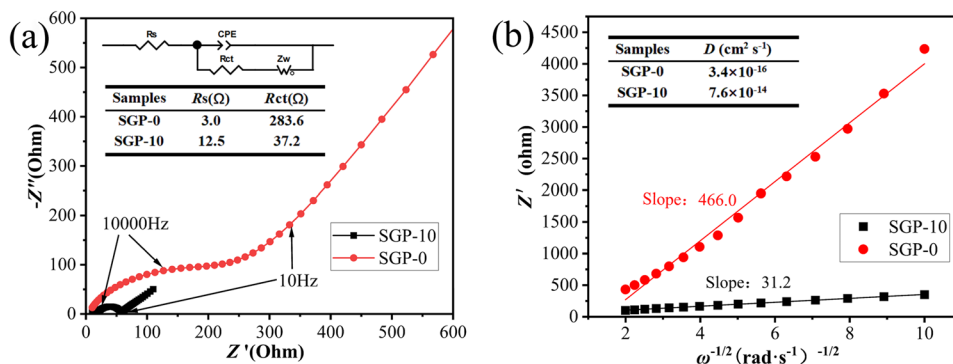
where  $a$  and  $b$  are variable parameters. The slope of the  $\log(v)$ - $\log(i)$  curve can be used to calculate the value of  $b$ . When the  $b$  value is equal to 1, the lithium storage

is controlled by a capacitance process; when the value of  $b$  is 0.5, the lithium storage is mainly characterized as a diffusion-controlled process [35]. The fitting results in Fig. 4c show that the  $b$ -values for the anode peak and cathode peak are 0.71 and 0.99, respectively, so the lithium storage process of the material is mainly influenced by capacitance. According to Formula (3), the contribution rates of capacitance and diffusion behaviors can be quantitatively calculated.

$$i(v) = k_1v + k_2v^{1/2} \quad (3)$$

Among them,  $k_1v$  and  $k_2v^{1/2}$  represent the pseudocapacitance control and diffusion control processes, respectively. Figure 4d shows the fitting profile of the pseudocapacitance and diffusion contributions at a scan rate of 0.8 mV s<sup>-1</sup>. Figure 4e shows that the pseudocapacitance contribution gradually increases from 60 to 92% with the increase of scan rate from 0.1 to 0.8 mV s<sup>-1</sup>. This phenomenon suggests that the lithium storage behavior of Si/graphite/C materials is primarily controlled by the pseudocapacitance. The carbon cage structure provides additional Li<sup>+</sup> adsorption sites which plays an important role in improving the pseudocapacitive behavior [36].

**Fig. 5** **a** Impedance plots of the SGP-0 and SGP-10 samples with the inset figure corresponding to the equivalent circuit. **b** Plot of  $Z'$  vs.  $\omega^{-1/2}$  at low frequency



Nyquist diagrams of the SGP-0 and SGP-10 anode materials are shown in Fig. 5a. The impedance spectra are fitted according to the equivalent circuit (inset) using the ZWinSimp software. The semicircles in the high frequency regions correspond to the charge transfer resistances ( $R_{ct}$ ), and the oblique straight lines in the low frequency region relate to the Warburg impedances ( $Z_w$ ) coming from the solid-phase diffusion of  $\text{Li}^+$  into the electrode material. The  $R_{ct}$  values of SGP-0 and SGP-10 were 283.6 and 37.2  $\Omega$  respectively after activation. This significant improvement benefits from the conductive interface between nano-Si and graphite, which is constructed from mesophase pitch-derived carbon. The diffusion coefficient was calculated by obtaining the Warburg coefficient ( $\sigma$ ) through the following equation [37–39]:

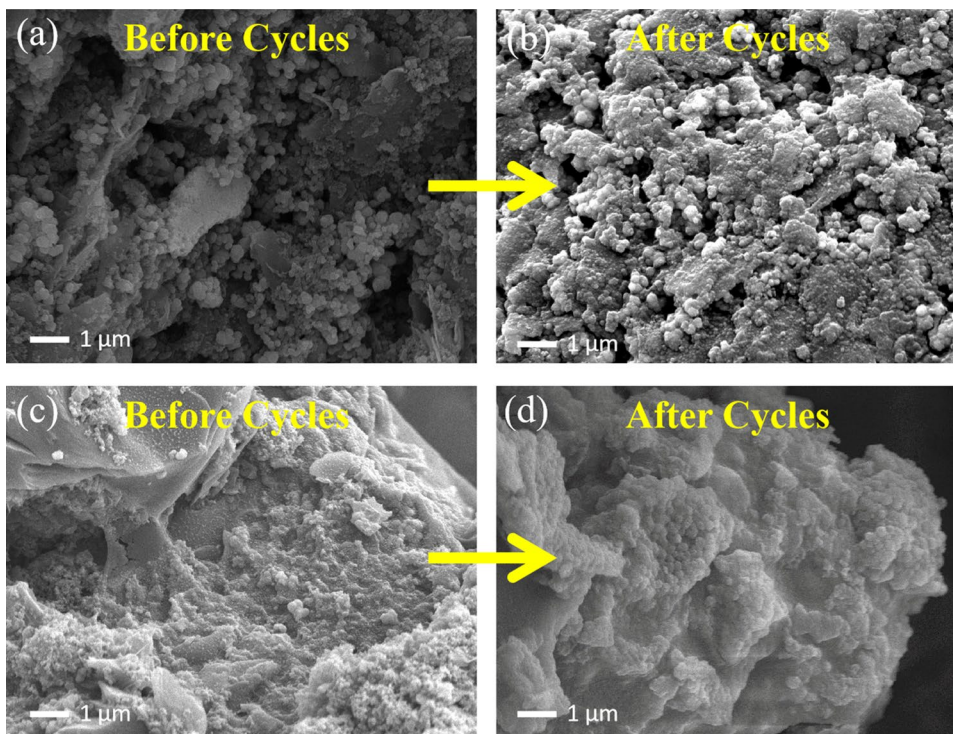
$$D_{\text{Li}^+} = \frac{R^2 T^2}{2A^2 n^4 F^4 C^2 \sigma^2} \tag{4}$$

$$Z' = R_s + R_{ct} + \sigma \omega^{-1/2} \tag{5}$$

where  $R$  is the ideal gas constant,  $T$  is the temperature in Kelvin,  $F$  is Faraday's constant,  $A$  represents the electrode surface,  $C$  is the concentration of  $\text{Li}^+$  in the electrode,  $\omega$  is the angular frequency,  $\sigma$  is the Warburg coefficient, and  $D_{\text{Li}^+}$  is the diffusion coefficient. From the slope ( $\sigma$ ), the  $D_{\text{Li}^+}$  values for the modified SGP-0 and SGP-10 electrodes were calculated to be  $3.4 \times 10^{-16}$  and  $7.6 \times 10^{-14} \text{ cm}^2 \text{ s}^{-1}$ , respectively. The results show that the ionic diffusion rate of SGP-10 is higher than that of SGP-0 due to the fast diffusion channels for lithium ions constructed by the pitch-derived carbon (Fig. 5b).

SEM images of the SGP-0 and SGP-10 electrodes before and after cycling are shown in Fig. 6. The unencapsulated silica nanoparticles showed severe chalking and agglomeration after 500 cycles (Fig. 6a–b). In contrast, the SGP-10

**Fig. 6** SEM images of SGP-0 and SGP-10 anode. **a, c** Before cycling and **b, d** after cycling



composite maintained structural integrity, indicating that the carbon cage has an excellent buffering effect on the stabilization of silicon particles (Fig. 6c–d). Overall, the high stability of the anode structure is of great significance for further improving the cycle life of the battery.

## Conclusion

In summary, a facile method for preparing carbon-caged Si/graphite anode materials for lithium-ion batteries, using naphthalene-based mesophase pitch as the carbon precursor, is proposed. The graphitizable carbon cage not only facilitates the diffusion of lithium ions, but also buffers the volume expansion during the lithiation of silicon nanoparticles. As a result, the Si/graphite/C anode material exhibited a specific capacity of 432 mAh g<sup>-1</sup> and a coulombic efficiency of 99.5% after 500 charge–discharge cycles at a high current density of 1000 mA g<sup>-1</sup>. Therefore, we believe that this work will contribute to the development of Si-based anode materials with excellent rate capability and cycling life.

**Funding** The authors gratefully appreciate the financial support of the National Natural Science Foundation of China (No. 52172063), the Natural Science Foundation of Hunan Province (No. 2023JJ30017, 2023JJ30030), the Natural Science Foundation of Changsha (No. kq2208223), the National Undergraduate Innovation Training Program of China (No. 202110536005), and assistance of Dr. Lingjun Li and Dr. Kangyu Zou in completing the full cell test.

**Availability of data and material** The data supporting the results of this study are included within this article.

## Declarations

**Conflict of interest** The authors declare no conflict of interests.

## References

1. Yang R, Yin XC, Xiao R, Mu TS, Huo H, Zuo PJ, Ma YL, Cheng XQ, Gao YZ, Yin GP, Li Y, Du CY (2022) Layered porous silicon encapsulated in carbon nanotube cage as ultra-stable anode for lithium-ion batteries. *Chem Eng J* 431:133982
2. Lu XQ, Xu P, Song WJ, Zhou P, Liao MD, Zeng G, Hu XB, Li JX, Zhang MY, Huang QZ, Su Z (2023) Dual Carbon boosts silicon-based anodes for excellent initial coulombic efficiency and cycling stability of lithium-ion batteries. *J Alloy Compd* 938:168646
3. Chaudhari KN, Rajeev KK, Kim SK, Nersisyan HK, Kirakosyan A, Jang WS, Choi JH, Lee JH, Kim TH, Kim YH (2022) Performance enhancement of carbon-coated Si nanoparticles for lithium-ion batteries through the generation of lithophilic sites by a simple oxidation process. *Appl Surf Sci* 602:154361
4. Smrekar S, Bracamonte MV, Primo EN, Luque GL, Thomas J, Barraco DE, Leiva E (2020) A mapping of the physical and electrochemical properties of composite lithium-ion batteries anodes made from graphite, Sn and Si. *Batteries Supercaps* 3:1248–1256
5. Guo JG, Zhai W, Sun Q, Ai Q, Li J, Cheng J, Dai LN, Ci LJ (2020) Facilely tunable core-shell Si@SiO<sub>x</sub> nanostructures prepared in aqueous solution for lithium ion battery anode. *Electrochim Acta* 342:136068
6. Jin CX, Lai Q, Dan JL, Xu GJ, Yue ZH, Li XM, Sun FG, Huang HB, Zhou L, Wang L (2021) A novel scalable synthesis of high-rate performance silicon anode materials by liquid-phase coating doping method. *Appl Surf Sci* 540:148326
7. He Q, Wu QY, Wang XX, Fu ST, Huang SC, Tong SF, Cao YF, Liu Z, Wu MM (2021) An anode material for lithium storage: Si@N-, S-Doped carbon synthesized via in situ self-polymerization. *ACS Applied Energy Materials* 4:3555–3562
8. Li Q, Liu XS, Han X, Xiang YX, Zhong GM, Wang J, Zheng BZ, Zhou JG, Yang Y (2019) Identification of the solid electrolyte interface on the Si/C composite anode with FEC as the additive. *ACS Appl Mater Interfaces* 11:14066–14075
9. Yang Y, Lu ZJ, Xia J, Liu Y, Wang K, Wang X (2021) Crystalline and amorphous carbon double-modified silicon anode: towards large-scale production and superior lithium storage performance. *Chem Eng Sci* 229:116054
10. Shao R, Zhu F, Cao ZJ, Zhang ZP, Dou ML, Niu J, Zhu BN, Wang F (2020) Heteroatom-doped carbon networks enabling robust and flexible silicon anodes for high energy Li-ion batteries. *Mater Chem A* 8:18338–18347
11. Fan Z, Liu WR, Sun L, Nishio A, Szczęsny R, Lin YG, Okada S, Gregory DH (2023) Carbon-free conversion of SiO<sub>2</sub> to Si via ultra-rapid alloy formation: toward the sustainable fabrication of nanoporous Si for lithium-ion batteries. *ACS Appl Mater Interfaces* 15:36076–36085
12. Shan JN, Yang XF, Yan C, Chen L, Zhao F, Ju YG (2019) Promoting Si-graphite composite anodes with SWCNT additives for half and NCM811 full lithium-ion batteries and assessment criteria from an industrial perspective. *Frontiers in Energy* 13(4):626–635
13. Zhang Y, Cheng YQ, Song JH, Zhang YJ, Shi Q, Wang JX, Tian FH, Yuan S, Su Z, Zhou C, Wang Y, Yang S (2021) Functionalization-assistant ball milling towards Si/graphene anodes in high performance Li-ion batteries. *Carbon* 181:300–309
14. Yi Z, Wang WW, Qian Y, Liu XY, Lin N, Qian YT (2018) Mechanical pressing route for scalable preparation of microstructured/nanostructured Si/graphite composite for lithium ion battery anodes. *ACS Sustainable Chem Eng* 6(11):14230–14238
15. Lai J, Guo HJ, Wang ZX, Li XH, Zhang XP, Wu FX, Yue P (2012) Preparation and characterization of flake graphite/silicon/carbon spherical composite as anode materials for lithium-ion batteries. *J Alloy Compd* 530:30–35
16. Lee D, Kondo A, Lee S, Myeong S, Sun S, Hwang I, Song T, Naito M, Paik U (2020) Controlled swelling behavior and stable cycling of silicon/graphite granular composite for high energy density in lithium-ion batteries. *J Power Sources* 457:228021
17. Xu CJ, Shen L, Zhang WJ, Huang YL, Sun ZF, Zhao GY, Lin YB, Zhang QB, Huang ZG, Li JX (2023) Efficient implementation of kilogram-scale, high-capacity and long-life Si-C/TiO<sub>2</sub> anodes. *Energy Storage Mater* 56:319–330
18. Choi SH, Nam G, Chae S, Kim D, Kim N, Kim WS, Ma J, Sung J, Han SM, Ko M, Lee HW, Cho J (2019) Robust pitch on silicon nanolayer-embedded graphite for suppressing undesirable volume expansion. *Adv Energy Mater* 9:1803121
19. Hsu YC, Hsieh CC, Liu WR (2020) Synthesis of double core-shell carbon/silicon/graphite composite anode materials for lithium-ion batteries. *Surf Coat Technol* 387:125528
20. Liu WP, Xu HR, Qin HQ, Lv YL, Zhu GS, Lei XX, Lin F, Zhang ZJ, Wang LH (2020) Rapid coating of pitch to prepare carbon-encapsulated composites of nano-silicon and graphite for lithium battery anodes. *J Mater Sci* 55:4382–4394
21. Phadatar M, Patil R, Blomquist N, Forsberg S, Örtengren J, Hummelgård M, Meshram J, Hernández G, Brandell D, Leifer K,



- Sathyanath SKM, Olin H (2019) Silicon-nanographite aerogel-based anodes for high performance lithium-ion batteries. *Sci Rep* 9:14621
22. Liu P, Kong JR, Liu YR, Liu QC, Zhu HZ (2015) Graphitic mesoporous carbon based on aromatic polycondensation as catalyst support for oxygen reduction reaction. *J Power Sources* 278:522–526
  23. Xu Z, Du J, Feng C, He J, Li T, Jia H, Song K (2024) Constructing a buffer macroporous architecture on silicon/carbon anode for high-performance lithium-ion battery. *J Mater Sci: Mater Electron* 35(7):531
  24. Xie X, Xiao P, Pang L, Zhou P, Li Y, Luo J, Xiong J, Li Y (2023) Facile synthesis of yolk-shell Si/void/C nanoparticles with 3D conducting networks as free-standing anodes in lithium-ion batteries. *J Alloy Compd* 931:167473
  25. Huang XH, Guo RQ, Lin Y, Cao YQ, Wu JB (2022) Si/SiC/C in-situ composite microspindles as anode materials for lithium-ion batteries. *Electrochemical Acta* 422:140546
  26. Li H, Chen ZD, Kang ZR, Liu W, Chen YG (2023) High-density crack-resistant Si-C microparticles for lithium-ion batteries. *Energy Storage Materials* 56:40–49
  27. He YW, Ye ZB, Chamas M, Sougrati MT, Lippens PE (2021) Si/Cu-Zn(ox)/C composite as anode material for Li-ion batteries. *Solid State Ionics* 372:115774
  28. Hu XQ, Huang S, Hou XH, Chen HD, Qin HQ, Ru Q, Chu BL (2017) A Double Core-shell structure silicon carbon composite anode material for a lithium-ion battery. *SILICON* 10(4):1443–1450
  29. Batool S, Idrees M, Kong J, Zhang J, Kong S, Dong M, Hou H, Fan J, Wei H, Guo Z (2020) Assessment of the electrochemical behaviour of silicon/carbon nanocomposite anode for lithium-ion batteries. *J Alloy Compd* 832:154644
  30. Yang Z, Yang Y, Guo H, Wang Z, Li X, Zhou Y, Wang J (2018) Compact structured silicon/carbon composites as high-performance anodes for lithium-ion batteries. *Ionics* 24(11):3405–3411
  31. Huang Y, Li W, Peng J, Wu Z, Li X, Wang X (2021) Structure design and performance of the graphite/silicon/carbon nanotubes/carbon (GSCC) composite as the anode of a li-ion battery. *Energy Fuels* 35(16):13491–13498
  32. Chae S, Xu Y, Yi R, Lim HS, Velickovic D, Li X, Li Q, Wang C, Zhang JG (2021) A micrometer-sized silicon/carbon composite anode synthesized by impregnation of petroleum pitch in nanoporous silicon. *Adv Mater* 33(40):2103095
  33. Liu W, Xu H, Qin H, Lv Y, Zhu G, Lei X, Lin F, Zhang Z, Wang L (2019) Rapid coating of asphalt to prepare carbon-encapsulated composites of nano-silicon and graphite for lithium battery anodes. *J Mater Sci* 55(10):4382–4394
  34. Yang J, Wang Y, Li W, Wang L, Fan Y, Jiang W, Luo W, Wang Y, Kong B, Selomulya C (2017) Amorphous TiO<sub>2</sub> shells: a vital elastic buffering layer on silicon nanoparticles for high-performance and safe lithium storage. *Adv Mater* 29(48):1700523
  35. Shi H, Zhang W, Wang D, Wang J, Wang C, Xiong Z, Chen F-R, Dong H, Xu B, Yan X (2023) Facile preparation of silicon/carbon composite with porous architecture for advanced lithium-ion battery anode. *Journal Electroanal Chem* 937:117427
  36. Duan J, Kang K, Li P, Zhang W, Li X, Wang J, Liu Y (2024) The design and regulation of porous silicon-carbon composites for enhanced electrochemical lithium storage performance. *J Ind Eng Chem* 131:410–421
  37. Hsieh CC, Lin YG, Chiang CL, Liu WR (2020) Carbon-coated porous Si/C composite anode materials via two-step etching/coating processes for lithium-ion batteries. *Ceram Int* 46:26598–26607
  38. Hsieh CC, Liu WR (2020) Carbon-coated Si particles binding with few-layered graphene via a liquid exfoliation process as potential anode materials for lithium-ion batteries. *Surf Coat Technol* 387:125553
  39. Chen WT, Muruganantham R, Liu WR (2022) Construction of 3D porous graphene aerogel wrapped silicon composite as anode materials for high-efficient lithium-ion storage. *Surf Coat Technol* 434:128147

**Publisher's Note** Springer Nature remains neutral with regard to jurisdictional claims in published maps and institutional affiliations.

Springer Nature or its licensor (e.g. a society or other partner) holds exclusive rights to this article under a publishing agreement with the author(s) or other rightsholder(s); author self-archiving of the accepted manuscript version of this article is solely governed by the terms of such publishing agreement and applicable law.